Acta Cryst. (1984). A**40**, 515–522

Propagation of X-ray Beams in Distorted Crystals (Bragg Case). II. The Case of Strong Deformations

BY J. GRONKOWSKI* AND C. MALGRANGE

Laboratoire de Minéralogie–Cristallographie, Universités Pierre et Marie Curie (Paris VI) et Paris VII, Tour 16, 4 *place Jussieu*, 75230 *Paris CEDEX* 05, *France*

(*Received* 1 *August* 1983; *accepted* 12 *March* 1984)

Abstract

The creation of new wavefields in deformed crystals, a phenomenon widely recognized as responsible for some contrast features in X-ray topography, has been demonstrated analytically for the first time only very recently [Balibar, Chukhovskii & Malgrange (1983). *Acta Cryst.* A**39**, 387–399] in the case of a constant strain gradient. In the present paper it is shown by means of computer experiments (*i.e.* by solving Takagi's equations numerically) that the most important results of the theoretical approach can be readily extended to variable strain gradients. In particular, the conjecture is verified that the creation takes place only in the region of maximum curvature of the wavefield trajectory. Its relative intensity is shown to be equal to $\exp(-2\pi/|\alpha_0|)$, α_0 being proportional to the value of the strain gradient in that region. The utility of these results is demonstrated in a refined interpretation of the dislocation contrast in plane-wave reflection topography.

1. Introduction

X-ray propagation in crystals distorted by a small constant strain gradient was first studied by Penning & Polder (1961) in the transmission (Laue) case. In the previous paper (paper I) (Gronkowski & Malgrange, 1984), we have shown that Penning & Polder's theory can also be applied in the reflection (Bragg) case provided that the angle of incidence of the incident beam is chosen outside the total reflection range.

The first approach to the specific phenomena appearing in the case of strongly distorted crystals was made by Balibar (1969*a*, *b*) and Authier & Balibar (1970), who showed theoretically that new wavefields should be excited when the modulus of the constant strain gradient β was significantly larger than a critical value β_c. Then, Balibar, Epelboin & Malgrange (1975) studied the case of an incident pseudo-plane wave (*i.e.* a plane wave of finite lateral extent) impinging on a crystal distorted by a large constant strain gradient in the symmetric transmission case. By computer experiments based on Takagi's equations (Takagi, 1969) they were able to show that a wavefield propagating in the crystal with an intensity I_0 gives rise to a new wavefield in the area where the beam curvature is maximum, extracting an intensity

$$I = I_0 \exp(-\varepsilon/|\beta|) \tag{1}$$

out of the original wavefield. ε is a numerical factor determined from the results of the computer experiment.

Recently, Balibar, Chukhovskii & Malgrange (1983) (abbreviated as BCM) treated analytically the creation of new wavefields in the symmetric transmission case and a constant strain gradient β. They showed that the full form of (1) is

$$I = I_0 \exp(-2\pi\beta_c/|\beta|) \tag{2}$$

and that the creation of new wavefields is accompanied by interbranch scattering – wavefield 1 gives rise to a new wavefield of type 2 and reciprocally.

The aim of this paper is to show by means of computer experiments that BCM results can be applied in the Bragg case if the angle of incidence lies outside the total reflection range, that they can be confirmed numerically for variable strain gradient (§ 3) and finally that they can be used to explain some contrast features in reflection plane-wave topography (§ 4).

2. Theoretical

Let us first recall the formula for the strain-gradient function β

$$\beta = \frac{1}{kC(\chi_h\chi_{\bar{h}})^{1/2}\cos\theta_B}\,\frac{\partial^2(\mathbf{h}\,.\,\mathbf{u})}{\partial s_0\,\partial s_h}, \tag{3}$$

where $k = 1/\lambda$ is the wave vector, C is the polarization constant, θ_B is Bragg's angle, χ_h and $\chi_{\bar{h}}$ are the Fourier coefficients of the dielectric susceptibility, $\mathbf{u}$ is the displacement vector, $\mathbf{h}$ is the diffraction vector, s_h and

* Present and permanent address: Institute of Experimental Physics, Warsaw University, 00-681 Warsaw, Hoża Street 69, Poland.

0108-7673/84/050515-08$01.50

s_0 are the coordinates along the reflected and refracted directions, respectively.

The critical value β_c introduced by Authier & Balibar (1970) is

$$\beta_c = \pi/2\Lambda, \tag{4}$$

where

$$\Lambda = \lambda \cos\theta_B / C(\chi_h \chi_{\bar{h}})^{1/2} \tag{5}$$

is the extinction length.

A dimensionless parameter α (related to the parameter B of BCM) is introduced here

$$\alpha = \beta/\beta_c = 4B. \tag{6}$$

BCM presented their results in the special case of symmetric Laue geometry and they used the usual deviation parameter η. In fact, the parameter a defined by Gronkowski & Malgrange (1984), which characterizes the point on the dispersion surface regardless of the geometry, can be used as well and so the BCM results can be readily extended to all cases where beams can be defined, *i.e.* in the Laue geometry and in the Bragg case outside the total reflection range.

BCM obtained the wavefields propagating in the crystal through a Laplace integral of parabolic cylinder functions of two variables: the Laplace variable p and $p - 2i\beta x$. Because of the analogy between the two relations

$$p(x) = p - 2i\beta x \tag{7}$$

and

$$\eta(x) = \eta(0) + \beta x \tag{8}$$

[the latter written in the specific form for the symmetric Laue case, $\eta(0)$ being the value of η at the entrance surface and x the coordinate along the reflecting planes], they introduced the relation

$$p = -2i\eta(0). \tag{9}$$

Then (9) allows the interpretation of each component of the Laplace integral as a wave which propagates in the crystal for a given value of $\eta(0)$, *i.e.* a given incident plane wave.

In the general case (8) is replaced by equation (11) of paper I:

$$a(x) = a_i + \beta x, \tag{10}$$

where a_i is the value of a at the entrance surface. The last relation leads to $p = -2ia_i$ and the same interpretation of the Laplace components follows.

The parabolic cylinder functions can be interpreted using their asymptotic development which can be applied for large values of the variables (here $|a_i|$ and $|a_e|$, where a_e is the value of a at the exit point).

Under these assumptions the BCM results can be summarized as follows.

(i) If a does not change sign in the crystal (*i.e.* does not attain zero value), wavefields propagate according to geometrical optics theory. No new wavefield is created. Let us recall that $a = 0$ means the tie point at the apex of the dispersion surface and the energy flux parallel to the reflecting planes.

(ii) If a_e and a_i are of opposite signs, then a new wavefield is created in the area where $a = 0$, *i.e.* when the tie point attains the apex of the dispersion surface. The new wavefield takes a fraction $\exp(-2\pi|\alpha|)$ out of the initial intensity. This result is illustrated in Fig. 1. Whenever we have $a = 0$ along the wavefield trajectory a new wavefield is created with its tie point at the apex of the other branch of the dispersion surface (Fig. 2).

The computer calculations presented in § 3 were made to verify in the first place that the straightforward extension of the BCM results to the Bragg case, described above, was justified. This was verified for the simple case of a constant strain gradient β.

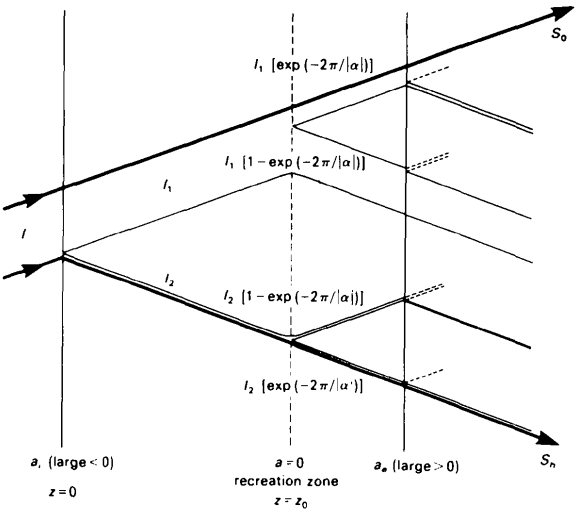

Fig. 1. Propagation of an incident parallel beam inside a crystal distorted by a constant strain gradient $\beta \gg \beta_c$. At the points where $a = 0$, along wavefields 1 and 2, a new wavefield is created taking a fraction $\exp(-2\pi/|\alpha|)$ of the intensity I_i ($i = 1, 2$) of the initial wavefield. β is here assumed to be positive.

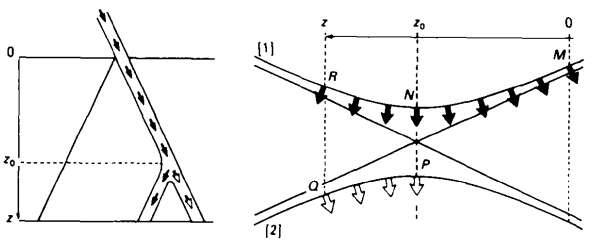

Fig. 2. Interbranch scattering (only one wavefield, here wavefield [1], has been pictured for clarity). At a depth z_0, the wavefield, which from $z = 0$ to $z = z_0$ propagates as a type [1] wavefield (black arrows from M to N), splits into two wavefields, one of type [1] (black arrows from N to R) and one of type [2] (white arrows from P to Q).

Secondly, if the BCM conjecture that a new wavefield is created exactly when $a=0$ was correct, then in the case of a variable strain gradient β the intensity fraction of this newly created wavefield should be equal to $\exp(-2\pi/|\alpha_0|)$, α_0 being the value of $\alpha=\beta/\beta_c$ at the point where a passes through zero. A numerical verification of this hypothesis is also described in § 3.

3. Computer experiments

As in paper I, Takagi's equations were solved numerically for a distorted crystal in the symmetric Bragg case with a narrow incident beam, using the same integration technique and boundary conditions. In contrast to paper I, however, the strain gradient was not small. Therefore, the propagation of the beam in the crystal, although still obeying the laws of geometrical optics (paper I, § 2), was accompanied by a non-negligible creation of new wavefields. Qualitatively this phenomenon was readily perceptible by eye in the maps of wavefield intensity inside the crystal (Fig. 3). In order to study it in a quantitative way we calculated numerically the integrated intensity of the newly created wavefield. The calculations were made first for a constant strain gradient β. Then β was made variable in such a way that it attained a chosen value β_0 at the point where the parameter a was equal to zero. The intensity of the newly created wavefield was then compared to that predicted by (2) with $\beta=\beta_0$. In this way, we were able to establish that the intensity of wavefield creation depended only on the value of β_0 and was insensitive to the β values in all other parts of the trajectory.

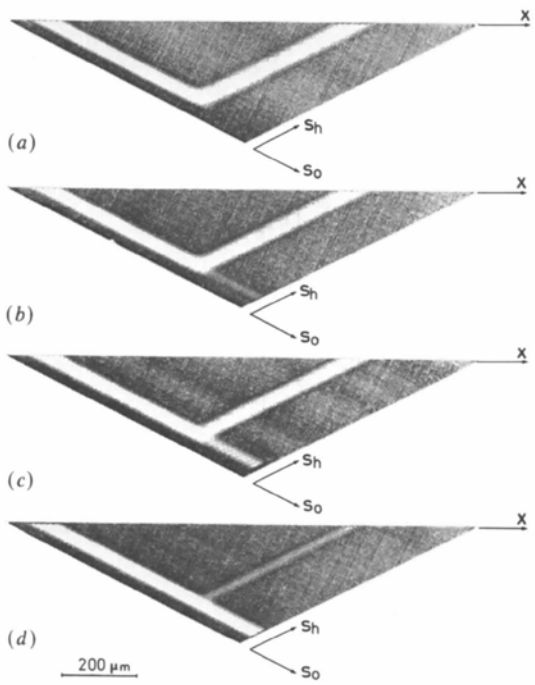

Fig. 3. Intensity distributions inside the crystal deformed with a strong constant strain gradient β: (*a*) $\beta=2\beta_c$, $\eta_i=-20$, (*b*) $\beta=3\beta_c$, $\eta_i=-30$, (*c*) $\beta=5\beta_c$, $\eta_i=-50$, (*d*) $\beta=40\beta_c$, $\eta_i=-400$. The intensity maps were printed on the Versatec half-tone printer using the procedure due to Epelboin (1978) (courtesy Y. Epelboin). Black means no intensity. Note how the intensity of the new wavefield (in the direction of $\mathbf{s}_0$) increases with β.

(*a*) *Constant strain gradient*

From paper I [§ 2, equation (17)], we know that in this case the trajectory of the beam is a hyperbola. In the Bragg case it is given by

$$\left(\frac{\beta z}{\tan\theta_B}+\eta_i\right)^2-[\beta x+S(\eta_i)(\eta_i^2-1)^{1/2}]^2=1. \quad (11)$$

If the signs of β and a_i are opposite then somewhere along the beam path a point is reached where $a=0$; we shall denote its coordinate by x_0. From equation (18) in paper I,

$$x_0=-S(\eta_i)(\eta_i^2-1)^{1/2}/\beta. \quad (12)$$

Let us recall that we consider only incident waves outside the total reflection range, *i.e.* $|\eta_i|>1$. The trajectory is deflected to the crystal surface which is reached at the point x_e:

$$x_e=2x_0. \quad (13)$$

The wavefields for which a_i is of the same sign as β do not pass through $a=0$ and are deflected to the inside of the crystal. If β is large the curvature of the trajectory in the vicinity of $a=0$ becomes very large and its hyperbolic shape degenerates into two straight lines respectively parallel to $\mathbf{s}_0$ and $\mathbf{s}_h$ directions joined by a small arc. The beam is then practically reflected within a small region situated inside the crystal.

A series of calculations for β values between $3\beta_c$ and $100\beta_c$ were made with the data corresponding to the symmetric Bragg 444 reflection in a silicon single crystal, for Mo $K\alpha_1$ radiation, neglecting absorption. The integrated intensity of the newly created wavefield was compared to that predicted by (2). The results are shown in Fig. 4 and in Table 1 (second and third columns); an excellent agreement is readily noted.

(*b*) *Variable strain gradient*

In a crystal deformed by a constant strain gradient the value of β is the same for each point of the trajectory. Consequently, intensity calculations in this case do not allow any conclusions to be drawn concerning an eventual influence of the tie-point position on the intensity of wavefield creation. A study of this dependence is possible if one deals with strain gradients which are a function of x. The form of this

function should be sufficiently simple for interpretation and easily adjustable through the choice of parameters. After some tests we found that a Lorentzian function was very suitable for such studies:

$$\beta(x)=\frac{A}{B}\frac{1}{1+[(x-x_m)/B]^2}, \tag{14}$$

where A and B are parameters and x_m determines the position of the maximum. The shape of this function is shown in Fig. 5; it is symmetrical with respect to $x=x_m$, it has a maximum there with $\beta_{\max}=\beta(x_m)=A/B$ and its half-width is equal to $2B$. On both sides of the peak it falls off quickly with $|x-x_m|$; for $|x-x_m|>4B$ the values of β do not exceed 6% of the maximum. Therefore, the choice of B determines the lateral range of the strain gradient while the choice of A decides the spread of β values.

The basic equation of the geometrical theory*

$$\mathrm{d}a=\beta\,\mathrm{d}x \tag{15}$$

integrated with $\beta(x)$ of (14) gives

$$a(x)=a_i+A\{\arctan[(x-x_m)/B]+\arctan[x_m/B]\}. \tag{16}$$

* Equation (5) of paper I.

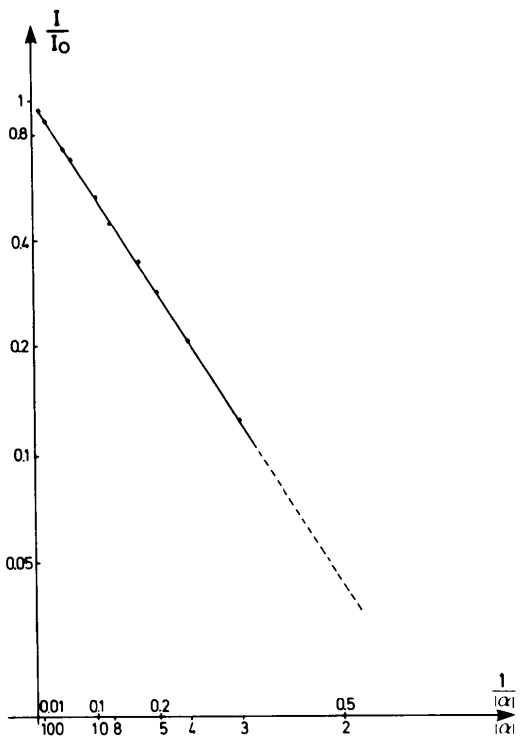

Fig. 4. Comparison of the intensity of new wavefield creation as a function of $|\alpha|$ predicted by (2) (solid line) and calculated from Takagi's equation (points).

In our calculations we fixed the value of x_m as 400 μm and that of B as 60 μm so that they were sufficiently larger than the step of integration which was equal to 1 μm. Then, by choosing appropriate values of A and a_i the dependence $a(x)$ could be adjusted so that:

1. $a=a(x)$ changed in such a way that the value $a=0$ was attained; we denote the coordinate of the

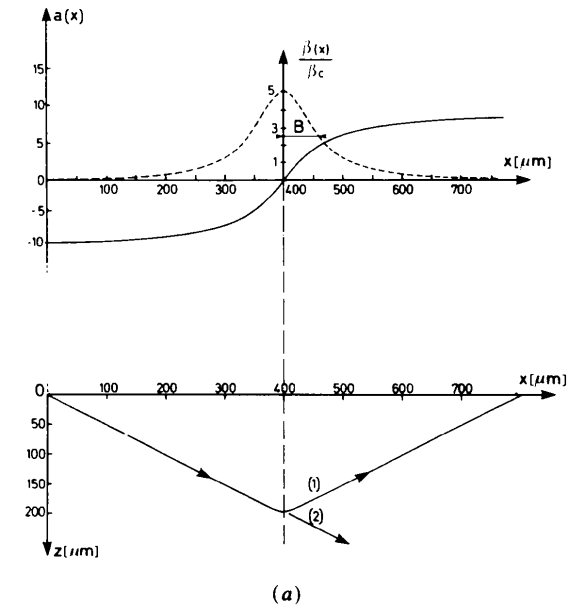

(a)

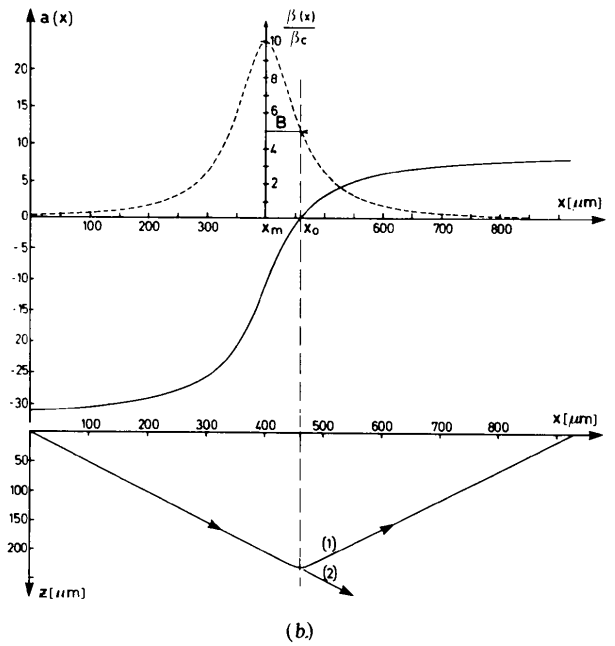

(b)

Fig. 5. The β function used in the computer experiments in the case of a variable strain gradient (upper row, broken line), the resulting shape of the function $a=a(x)$ (upper row, solid line) and trajectory (lower row). (*a*) $x_0=x_m$, (*b*) $x_0=x_m+B$, (*c*) $x_0=x_m-B$.

Table 1. *Comparison of the relative intensity I/I_0 of the newly created wavefield predicted by equation (2) (second column) and calculated from Takagi's equation for a constant strain gradient (third column) and a variable strain gradient, equation (14) (fourth to tenth columns)*

$\alpha_0 = \beta_0/\beta_c$; for other notations see § 3.

		Constant strain	Variable strain gradient						
$\lvert\alpha_0\rvert$	$\exp(-2\pi/\lvert\alpha_0\rvert)$	gradient	$x_0 = x_m$	$x_0 = x_m + B$	$x_0 = x_m - B$	$x_0 = x_m + 0{\cdot}5B$	$x_0 = x_m - 0{\cdot}5B$	$x_0 = x_m + 0{\cdot}25B$	$x_0 = x_m - 0{\cdot}25B$
3	0·1231	0·1252	0·1291	0·1347	0·1262	0·1346	0·1270	0·1317	0·1275
4	0·2079	0·2102	0·2107	0·2146	0·2093	0·2146	0·2096	0·2122	0·2098
5	0·2846	0·2869	0·2862	0·2891	0·2849	0·2890	0·2854	0·2870	0·2857
6	0·3509	0·3531	0·3518	0·3542	0·3510	0·3542	0·3513	0·3524	0·3516
8	0·4559	0·4579	0·4563	0·4580	0·4557	0·4581	0·4560	0·4565	0·4558
10	0·5334	0·5352	0·5337	0·5351	0·5332	0·5351	0·5334	0·5337	0·5335
12	0·5924	0·5941	0·5924	0·5936	0·5921	0·5936	0·5926	0·5924	0·5925
14	0·6383	0·6406	0·6384	0·6400	0·6381	0·6394	0·6387	0·6383	0·6382
16	0·6752	0·6796	0·6752	0·6760	0·6749	0·6761	0·6747	0·6751	0·6749
18	0·7053	0·7095	0·7053	0·7061	0·7050	0·7061	0·7050	0·7052	0·7053
20	0·7304	0·7341	0·7303	0·7310	0·7300	0·7310	0·7302	0·7302	0·7302
30	0·8110	0·8135	0·8108	0·8115	0·8105	0·8113	0·8108	0·8107	0·8109
40	0·8546	0·8564	0·8544	0·8547	0·8543	0·8548	0·8544	0·8543	0·8543
50	0·8819	0·8833	0·8816	0·8820	0·8815	0·8819	0·8816	0·8815	0·8816
60	0·9006	0·9017	0·9003	0·9005	0·9002	0·9005	0·9003	0·9002	0·9003
80	0·9245	0·9252	0·9241	0·9243	0·9241	0·9243	0·9241	9·9240	0·9240
100	0·9391	0·9396	0·9387	0·9390	0·9387	0·9388	0·9387	0·9386	0·9387

point where it happened by x_0:

$$a(x_0) = 0; \tag{17}$$

2. the value of β at this point was equal to a chosen value β_0

$$\beta(x_0) = \beta_0. \tag{18}$$

In the cases illustrated in Fig. 5 the parameters A and a_i were chosen in such a way that $a = 0$ for $x_0 = x_m$, $x_m + B$ and $x_m - B$ respectively, *i.e.* at the maximum of β and in both flanks. The corresponding values of

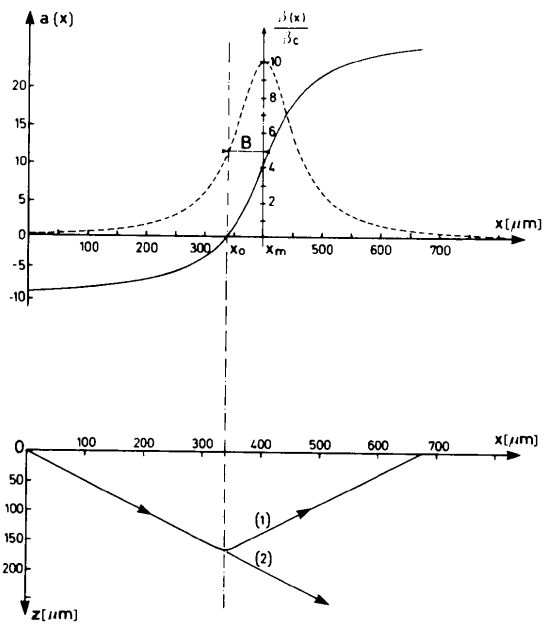

(*c*)

Fig. 5 (*cont.*)

β_0 were, however, the same in the three cases. The values of A and a_i which satisfy both (17) and (18) were determined in each case from the set of equations

$$a_i + A\{\arctan[(x_0 - x_m)/B] + \arctan[x_m/B]\} = 0 \tag{19a}$$

$$\frac{A}{B}\frac{1}{1+[(x_0-x_m)/B]^2} = \beta_0 \tag{19b}$$

obtained by substituting (16) into (17) and (14) into (18).

In the first series of calculations with a variable strain gradient the parameters A and a_i were chosen in such a way that $x_0 = x_m$, *i.e.* the tie point attained the apex of the dispersion surface at the same time as β attained its maximum ($\beta_0 = \beta_{max} = A/B$) (Fig. 5*a*). The calculations were made for a set of different values of β_0 between $3\beta_c$ and $100\beta_c$. The results are shown in Table 1 (fourth column).

Although the agreement between the calculated and expected intensities is again very good, this series of results does not provide a definitive support to the thesis that the wavefield creation takes place only when $a = 0$. It could be as well concluded that it is simply the maximum value of β anywhere along the beam path which decides the intensity. Consequently, the results of the first series could not be treated as conclusive.

A firmer conclusion can be reached if we choose $x_0 = x_m \pm B$ (*i.e.* the point where $a = 0$ is reached at the same time as the middle of one of the flanks of the β distribution, with $\beta_0 = 0{\cdot}5\beta_{max} = A/2B$, see Figs. 5*b*, *c*).

The results of the calculations in this series, shown in Table 1 (fifth column for $x_0 = x_m + B$ and sixth

column for $x_0 = x_m - B$) are again in very good agreement with the values predicted for $\beta = \beta_0$. Consequently, they indicate that the maximum value of β is of no importance. However, they do not allow us to exclude the interpretation that it is the average value $\langle\beta\rangle$ over a certain section of the beam path (*e.g.* corresponding to $-1 < a < +1$) which determines the intensity of the new wavefields, since $\langle\beta\rangle$ in this series was always very near to β_0.

In order to avoid this ambiguity of interpretation we repeated the calculations also for two other choices of x_0, namely $x_0 = x_m \pm 0{\cdot}5B$ and $x_0 = x_m \pm 0{\cdot}25B$. Then, the average values $\langle\beta\rangle$ for $-1 < a < 1$ differed significantly from the respective value of β_0. The results for these series are shown in the last four columns of Table 1.

In all these calculations, regardless of the choice of x_0, we obtained a very good agreement with the theoretical values of the intensity. Therefore, we are able to conclude that it was indeed the value of the strain gradient β in the immediate vicinity of the point where $a = 0$ which determined the intensity of the phenomenon of new wavefield creation.

4. Application to the case of a screw dislocation

As an example of practical application of the approach presented in §§ 2 and 3 we shall discuss the case of a screw dislocation normal to the crystal surface. This case was treated theoretically by Bedynska (1973) who obtained for the first time simulations of defect contrast in the Bragg case by solving numerically Takagi's equations. With remarkable experimental skill Bubákova & Sourek (1976) succeeded in demonstrating the fine fringe structure of the contrast, predicted by Bedynska's simulations. The fringe distances in their topographs, equal to those in the simulations (Bedynska, Bubákova & Sourek, 1976) were in perfect agreement with the simple formula derived in the theoretical explanation of the origin of the fringes (Bedynska, 1978). We shall show that by applying an analysis similar to that of § 3, based on geometrical optics and BCM results [equation (2)], it has now become possible also to explain some other features of Bedynska's contrast which were inexplicable without such an approach. Bedynska, Bubákova & Sourek (1976) obtained plane-wave topographs in the double-crystal arrangement for five different incidence angles corresponding to $|\eta_i|$ between 1 and 1·5 in our notation and compared them to computer simulations. The topographs and (more distinctly) the simulations presented characteristic fringes, besides the principal black and white contrast known from previous works [notably those of Bonse (1958) and Renninger (1965)]. A typical simulation is shown in Fig. 6 (courtesy T. Bedynska). According to Bedynska's model (Bedynska, 1978), the fringes visible on all simulations arise as a result of interference between the incident wave and the new wavefields created in the vicinity of the dislocation core where the strain gradient is large. Since the difference $|\Delta\mathbf{K}_x|$ in the wave-vector components parallel to the surface between the interfering waves is

$$|\Delta\mathbf{K}_x| = |\eta_i|/\Lambda \tag{20}$$

(in our notation), the fringe distances along the surface are easily calculated as

$$\Delta x = \Lambda/|\eta_i|, \tag{21}$$

in full accordance with those measured in the simulations and topographs.

Two features of the images could not be explained, however, by this model:

(i) *The lateral extent of the fringes*

In order to estimate the value of y (the coordinate normal to the plane of incidence) for which fringes should cease to be visible, Bedynska (1978) assumed that the strain gradient should not exceed the critical value β_c:

$$|\beta| < \beta_c. \tag{22}$$

Since in this case β is a function of x with y as a parameter

$$\beta(x) = -\frac{b \sin 2\theta_B}{\pi(\chi_h\chi_{\bar{h}})^{1/2}} \frac{xy}{(x^2+y^2)^2}, \tag{23}$$

where b is the length of the Burgers vector (we assume $C = 1$) and $|\beta|$ attains maximum values $\beta_{\max}$ for $x_m = \pm y/\sqrt{3}$,

$$\beta_{\max} = \frac{b \sin 2\theta_B}{\pi(\chi_h\chi_{\bar{h}})^{1/2}} \frac{9}{16\sqrt{3}} \frac{1}{y^2}, \tag{24}$$

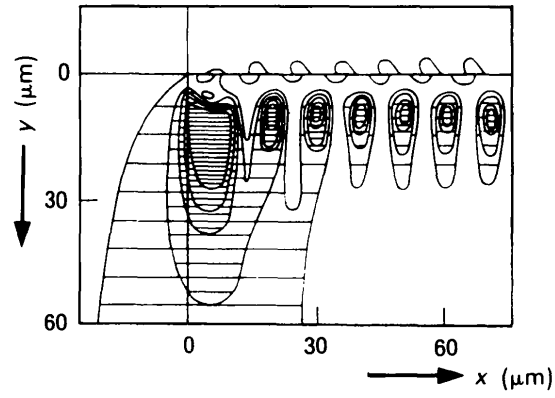

Fig. 6. The intensity distribution on the crystal surface calculated by Bedynska, Bubákova & Sourek (1976) (courtesy T. Bedynska). Si 422 reflection, Mo $K\alpha_1$ radiation, $\eta_i = -1{\cdot}5$. Note that the fringes are the most intense about 10 μm from the line $y = 0$, *i.e.* the plane of incidence containing the dislocation line.

the condition (22) gives for this case

$$|y| > 18{\cdot}5\ \mu\text{m}.$$

This limiting value of 18·5 μm is independent of η_i. However, in some of the simulations oscillations of the intensity were still visible for $|y|$ exceeding 30 μm.

(ii) *The intensity of the fringes*

The maximum intensity of the fringes is obtained in the planes of incidence for which y is clearly far from zero, for instance about 10 μm for $\eta_i = -1{\cdot}49$ (Fig. 6). At the same time the value of y corresponding to the maximum fringe intensity depends on the value of η_i.

Neither of these effects could be explained by Bedynska's model.

In order to explain (i) we shall integrate for $|\eta_i| > 1$ the basic equation of the geometrical theory (15) with β given by (23). The integration gives the following dependence $a = a(x)$.

$$a = a_i + \frac{yb \sin 2\theta_B}{2\pi(\chi_h\chi_{\bar{h}})^{1/2}}\left(\frac{1}{x^2+y^2} - \frac{1}{x_i^2+y^2}\right) \quad (25)$$

with $a_i = S(\eta_i)(\eta_i^2-1)^{1/2}$ and x_i the coordinate of the point of incidence of the beam. Fig. 7 shows the shape of a for a chosen set of parameters a_i, x_i and y together with $\beta = \beta(x)$ and the resulting trajectory. Creation of new wavefields should take place wherever $a = 0$ with the intensity given by (2). Now, a can attain the zero value if $\max(|a - a_i|) > |a_i|$ equivalent to $|a(0) - a_i| > |a_i|$, which can be satisfied only if

$$|y| < \frac{b \sin 2\theta_B}{2\pi(\chi_h\chi_{\bar{h}})^{1/2}} \frac{1}{(\eta_i^2-1)^{1/2}}$$

(we assume $x_i^2 \gg y^2$).

For the case in question this condition gives, for example, $|y| < 50$ μm for $|\eta_i| = 1{\cdot}1$, $|y| < 34{\cdot}6$ μm for $|\eta_i| = 1{\cdot}2$ and $|y| < 20{\cdot}6$ μm for $|\eta_i| = 1{\cdot}5$. These values are in better accord with the simulated images of Bedynska, Bubákova & Sourek (1976) than the value of 18·5 μm evaluated above.

As to the problems in (ii), they can be resolved by a careful examination of the trajectory (Fig. 7*b*) in the case when a attains zero. There are two such points on the trajectory, A_1 and A_2 (Fig. 8). Besides, the new wavefield created at A_1 also has one point (A_3) where $a = 0$ since it propagates according to geometrical theory, symmetrically to the original wavefield. All these three points have the same absolute value $|x_0|$ of the x coordinate and consequently the same value of $|\beta_0|$.

Therefore, the phenomenon of new-wavefield creation is equally intense in each of them and it obeys (2). Applying (2) successively in A_1, A_2 and A_3 we obtain for the intensity of new wavefields arriving at the crystal surface

$$I = I_4 + I_5 = 2I_0 \exp\left(-\frac{2\pi\beta_c}{|\beta_0|}\right)\left[1 - \exp\left(-\frac{2\pi\beta_c}{|\beta_0|}\right)\right].$$

It attains its maximum when

$$\exp(-2\pi\beta_c/|\beta_0|) = 0{\cdot}5$$

or

$$|\beta_0| = 9{\cdot}06\beta_c.$$

Therefore, the fringes should be most intense in those cases when the value $|\beta_0|$ of the strain gradient (at the point where $a = 0$ is reached) happens to be equal to $|\beta_0| = 9{\cdot}06\beta_c$. For a given incidence parameter η_i the value of y for which such a coincidence takes

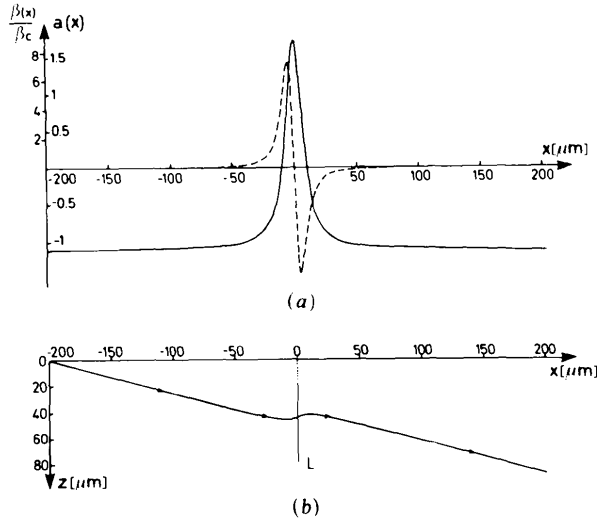

Fig. 7. The case of a screw dislocation normal to the crystal surface (Bedynska, Bubákova & Sourek, 1976) from the view-point of geometrical optics of X-rays. (*a*) The function $\beta = \beta(x)$ (broken line) and $a = a(x)$ (solid line); (*b*) the resulting ray trajectory. L is the projection of the dislocation on the incidence plane. Si 422 reflection, Mo $K\alpha_1$ radiation, $\beta_c = 0{\cdot}0327$ [μm^{-1}], $x_i = -200$ μm, $\eta_i = -1{\cdot}5$, $y = 8$ μm.

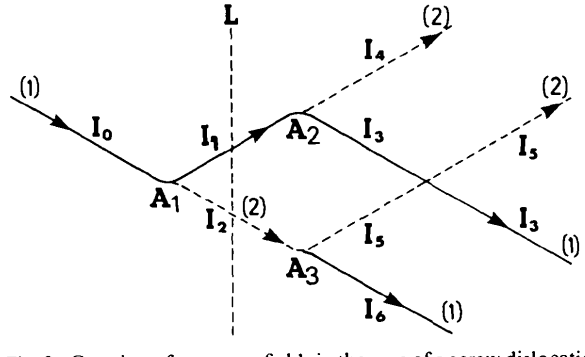

Fig. 8. Creation of new wavefields in the case of a screw dislocation normal to the surface. Solid line – wavefield (1), broken line – wavefield (2). A_1, A_2 and A_3 – points where $a = 0$; L is the projection of the dislocation line on the incidence plane.

place can be determined from the following set of equations:

$$|\beta(x_0)| = 9{\cdot}06\beta_c$$

$$a(x_0) = S(\eta_i)(\eta_i^2 - 1)^{1/2} + \frac{yb \sin 2\theta_B}{2\pi(\chi_h\chi_{\bar{h}})^{1/2}}\left(\frac{1}{x_0^2+y^2} - \frac{1}{x_i^2+y^2}\right) = 0.$$

In this way we may obtain the theoretical dependence of the y of maximal fringe intensity on η_i. Indeed, by solving the above set of equations we readily obtained the same type of dependence of the maximum fringe intensity that can be seen in the simulations. The agreement is, however, only qualitative. This is because the wavefields (I_4 and I_5) arriving at the crystal surface interfere. Certainly, it is also an important factor that the region where the trajectories change dramatically and wavefield creation takes place is quite small ($2|x_0|$ of the order of 20 μm) compared with the wave-front width in the real topographic conditions where a plane wave was employed.

5. Conclusion

In this paper a very important result concerning X-ray propagation has been obtained: geometrical optics results can be used if one takes into account the creation of new wavefields which occurs along every beam trajectory at the point where $a = 0$ with an intensity directly related to the value of the strain gradient at this point. This result has been demonstrated here in the Bragg case but it is general enough to be valid also in the Laue case.

Such an 'extended' geometrical-optics treatment when applied to any practical type of distortion, *e.g.* a dislocation line, should lead to a better understanding of the contrast origin in X-ray topographs.

As pointed out, geometrical optics cannot be applied in the total reflection range of the Bragg case. It seems, however, that there should be a similarity between the mechanism of the new wavefield creation in strongly deformed crystals and the phenomena occurring during total reflection. In this respect, it is obviously worthwhile to study this mechanism in more detail.

The authors wish to thank Dr Bedynska for her consent to reproduce here one of her simulations (Fig. 6). They are also grateful to Dr Y. Epelboin whose representation routine was a helpful tool for the visualization of the phenomenon of new-wavefield creation (Fig. 3). One of us (JG) acknowledges the financial support of CNRS for subsidizing a one-year stay at the Laboratoire de Minéralogie–Cristallographie in Paris.

References

AUTHIER, A. & BALIBAR, F. (1970). *Acta Cryst.* **A26**, 647–654.
BALIBAR, F. (1969*a*). *Acta Cryst.* **A25**, 650–658.
BALIBAR, F. (1969*b*). Thesis, Paris.
BALIBAR, F., CHUKHOVSKII, F. N. & MALGRANGE, C. (1983). *Acta Cryst.* **A39**, 387–399.
BALIBAR, F., EPELBOIN, Y. & MALGRANGE, C. (1975). *Acta Cryst.* **A31**, 836–840.
BEDYNSKA, T. (1973). *Phys. Status Solidi*, **A18**, 147–154.
BEDYNSKA, T. (1978). Dissertation, Warsaw (in Polish).
BEDYNSKA, T., BUBÁKOVA, R. & SOUREK, Z. (1976). *Phys. Status Solidi*, **A36**, 509–516.
BONSE, U. (1958). *Z. Phys.* **153**, 278–296.
BUBÁKOVA, R. & SOUREK, Z. (1976). *Phys. Status Solidi*, **A35**, 55–60.
EPELBOIN, Y. (1978). *J. Appl. Cryst.* **11**, 675–680.
GRONKOWSKI, J. & MALGRANGE, C. (1984). *Acta Cryst.* **A40**, 507–514.
PENNING, P. & POLDER, D. (1961). *Philips Res. Rep.* **16**, 419–440.
RENNINGER, M. (1965). *Z. Angew. Phys.* **19**, 20–35.
TAKAGI, S. (1969). *J. Phys. Soc. Jpn*, **26**, 1239–1253.

Acta Cryst. (1984). A**40**, 522–526

A Matrix Basis for CBED Pattern Analysis

BY P. GOODMAN

CSIRO, Division of Chemical Physics, Melbourne, Australia

(*Received* 31 *July* 1983; *accepted* 4 *April* 1984)

Abstract

A simple construction procedure is given for convergent-beam electron diffraction (CBED) pattern matrices as symmetry elements in diffraction space coordinates. These are constructed from a limited set of point-group elements, namely those belonging to the layer groups of Alexander & Hermann [*Z. Kristallogr.* (1929), **70**, 328–345]. As a result a transformation is found between crystal and diffraction space in which the three-dimensional crystal symmetries transform into four-dimensional intensity distributions. Equivalent anti-symmetric matrices which operate on amplitudes rather than intensities are found for non-symmorphic space-group elements.

0108-7673/84/050522-05$01.50